MULTIPLE ANTENNA MICROWAVE ABLATION: IMPACT OF NON-PARALLEL ANTENNA INSERTION

by

SOUVICK MUKHERJEE

B. Tech West Bengal University of Technology

A THESIS

submitted in partial fulfillment of the requirements for the degree

MASTER OF SCIENCE

Department of Electrical and Computer Engineering
College of Engineering

KANSAS STATE UNIVERSITY
Manhattan, Kansas

2015

Approved by:

Major Professor
Dr. Punit Prakash

ABSTRACT

Microwave ablation is a minimally invasive therapeutic modality used for the treatment of cancer in various organs. In this procedure, microwave energy is sent through a thin antenna placed inside the tumor. The microwave energy radiated from the antenna generates heat which kills the tumor cells by necrosis. During multiple-applicator microwave ablation, geometric estimates of treatment outcome are typically obtained by assuming parallel insertion of the applicators. This assumption is based on the guidelines provided in the brochures of antenna manufacturing companies. This assumption is flawed because it is rare to insert the antennas in parallel configuration due to the flexible nature of the antennas and the presence of intervening organs. Furthermore, movement of patients during the treatment procedure alters the position of the antennas. In order to see the effect of non-parallel insertion of antennas, model-based treatment planning may be instructive. Treatment planning can also determine the changes needed to be made for prospective ablation therapy if the antennas are not positioned in their ideal parallel configuration. This thesis provides a detailed computational comparison of the skewed configurations of microwave antennas to their closest parallel configurations. The metric used for comparing the similarity between the cases is Dice Similarity Coefficient (DSC). Experimental results to validate the computational data are also discussed. Computations were done by using realistic cases of antenna positions obtained from Rhode Island Hospital.

ACKNOWLEDGEMENTS

I would like to thank my advisors Dr. Punit Prakash, Dr. Bala Natarajan and Dr. Nathan Albin for providing ideas for this research. I would also like to thank Dr. Sergio Curto and Dr. Punit Prakash for helping me to conduct the experimental part of this research.

Finally but most importantly I would like to thank my family and all my friends for always being there for me during tough times.

CONTENTS

LIST OF FIGURES

LIST OF TABLES

CHAPTER 1: INTRODUCTION

Background and motivation

Cancer is a major worldwide public health problem. In the United States alone, 1,665,540 new cancer cases and 585,720 cancer deaths were envisioned to occur in 2014 [1]. One of every four deaths in the US is cancer-related. Figure 1.1 illustrates the cancer sites that are the most dangerous in terms of having the highest death rates. In this thesis, we focus our attention on minimally-invasive technologies for treating hepatocellular carcinoma (liver cancer) and lung cancer.

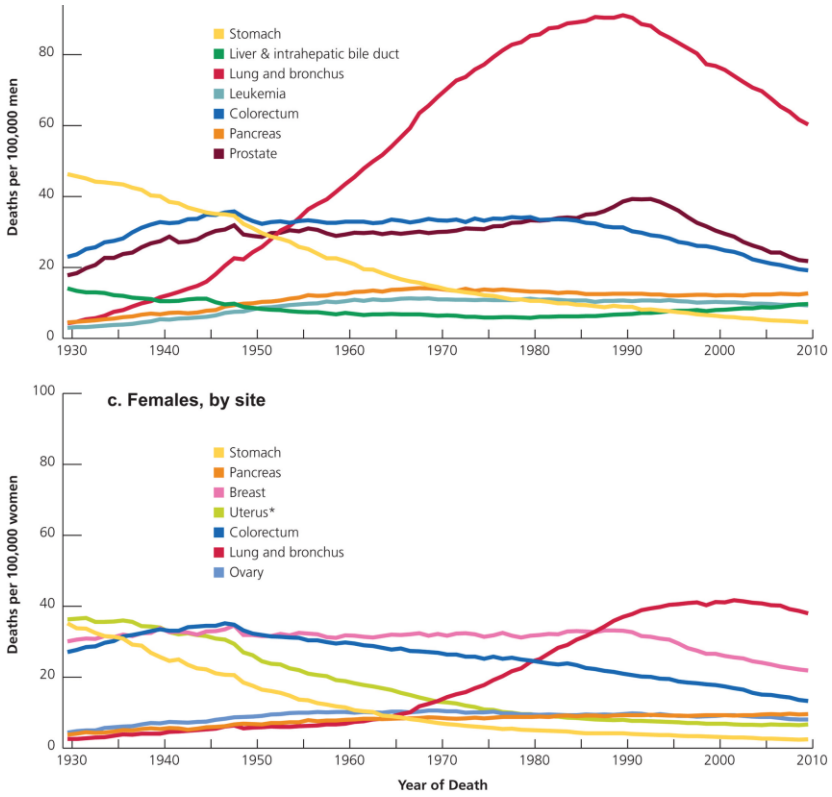

Figure 1.1. Trends in death rate by location of cancer in males and females [1].

Surgery is a preferred treatment method for patients with early stage cancer but not for advanced or metastatic disease which has grown into blood vessels. Surgery is not an option for

patients if it hinders the functional capability of an organ after resection. Organ transplant is another potential option, but comes at a large expense and finding a suitable organ donor, which is not always possible. Chemotherapy is not suitable for selective treatment of target tissues as it comes with a large risk of damaging healthy tissues [2]. Furthermore, chemotherapy has proven to be ineffective for treating liver cancer as the cancerous tissues resist the chemotherapeutic drugs. Ionizing radiation therapy uses high energy radiation to kill cancer cells by damaging their DNA. Radiation therapy poses a risk of damaging the DNA of healthy tissues in the vicinity of the tumor tissues [3]. There is a need to develop minimally-invasive treatments for treatment of surgically-unresectable localized tumors.

Thermal ablation is a minimally-invasive technique where tumor tissues are killed by exposing them to intense temperatures. During an ablation treatment, an applicator is inserted into the target organ under image guidance. Energy deposited by the applicator within tissue leads to heating, resulting in cell death at elevated temperatures. Figure 1.2 illustrates the objective of an ablation procedure, which is to ablate the target tumor together with a 10 mm margin of healthy tissue surrounding the tumor. This is done in order to decrease the chances of tumor recurrence.

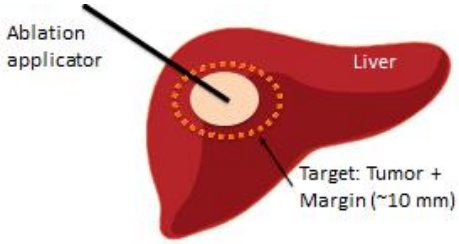

Figure 1.2. Illustration of a minimally-invasive ablation procedure

Among the several energy modalities available for thermal ablation, radiofrequency ablation (RF) is the most widely used in clinical applications. Other energy modalities for thermal

ablation include ultrasound [4], lasers [5], and microwaves [6]. During RF ablation, an active electrode is inserted at the target site, and an alternating current (460 kHz) is passed between this electrode and a distant, dispersive ground electrode. RF heating requires an electrically conductive path between two electrodes. As tissue temperature rises and the tissue desiccates and chars, the impedance at the electrode-tissue interface rises, thereby limiting the ablation process.

Compared to RF heating, microwaves offer greater volumetric heating, larger tissue temperatures and allow the synchronous operation of multiple applicators [7]. During microwave ablation, an antenna is inserted under image guidance, and radiates electromagnetic energy into the target tissue. As the electromagnetic wave oscillates, generally at 915 MHz or 2.45 GHz, water and other polar molecules also oscillate, leading to heat generation as a result of large frictional interaction between the water molecules. The two most widely used frequencies for microwave ablation devices are 915 MHz and 2.45 GHz.

Microwave propagation through lossy media

Microwaves are a form of electromagnetic radiation with frequencies ranging from 300 MHz to 300 GHz. Microwave propagation through a medium is governed by the electromagnetic wave equation. The electromagnetic wave gets attenuated as it passes through the tissue. A part of the wave gets absorbed into the medium, a part of it gets reflected back to the source and the rest of it gets transmitted. The propagation constant describes the behavior of an electromagnetic wave along a transmission medium. The propagation constant is $\gamma=\alpha+j\beta$ where α is the attenuation constant and β is the phase constant. The real part of propagation constant is the attenuation constant which causes the signal amplitude to decrease along the transmission path. The phase constant is the imaginary component of the propagation constant which determines the sinusoidal phase of the signal along the transmission medium at a constant time. Thus

depending on the attenuation constant in the tissue a part of the energy of the wave gets attenuated and absorbed in the medium. Figure 1.2 shows the composite effect of attenuation constant and phase constant in wave propagation. It shows wave propagation in a lossy medium with the attenuation constant α=0.05, and the phase constant β=1.

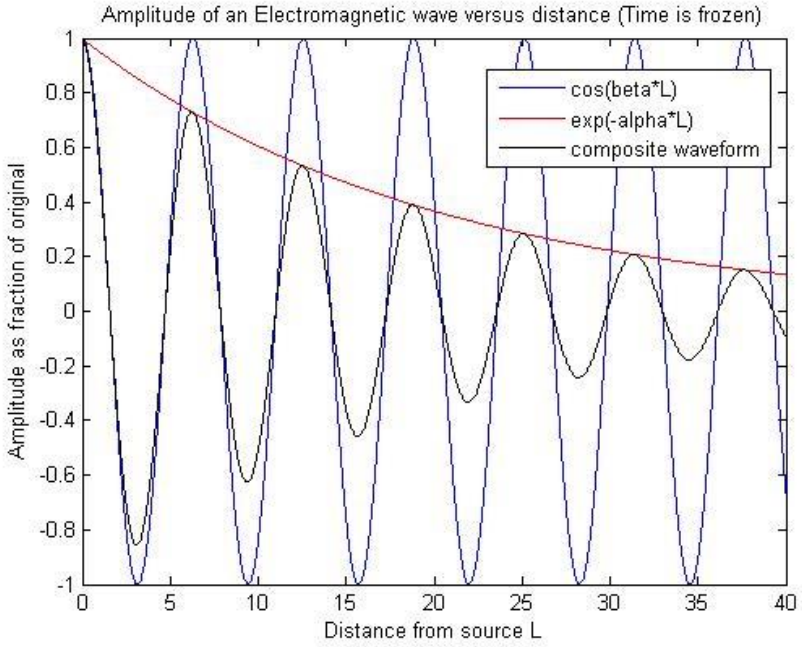

Figure 1.3. The propagation of wave in a lossy medium with α=0.05 and β=1.

Although the cell damage due to heating is a complex process, the level of thermal damage following an ablation procedure can be approximated by the first order chemical kinetics reaction process governed by the Arrhenius equation.

$$\Omega(t) = ln(c(0)/c(t)) = \int_0^t A \cdot e^{-\frac{\Delta E}{RT}} dt \quad (1)$$

Where Ω(t) is the degree of tissue injury, c(t) is the concentration of living cells, c(0) is the initial concentration of living cells, R is the universal gas constant, A is a "frequency" factor for the kinetic expression (s^{-1}), and ΔE is the activation energy for the irreversible damage reaction ($J\text{-}mol^{-1}$). Ω=1 signifies the point where thermal necrosis occurs, i.e. when 37% of the cells are

alive and 63% of the cells are killed by tissue necrosis. The Arrhenius equation gives us an estimate of the percentage of cell survivability, Ω=4.6 indicates a probability of 99% cell death during ablation. For complete ablation of the target tissue the values of the parameters in Arrhenius equation are set to the following: $\Omega=4.6$, $A = 7.39 \times 10^{39}\ s^{-1}$ and $\Delta E = 2.577 \times 10^{5}\ J\text{-}mol^{-1}$ [8]

By using these values and solving equation (1) above recursively for different values of temperature starting from the normal body temperature of 37 °C we can observe that for complete ablation of target volumes we need to heat the target tissues at approximate temperatures of about 60 °C for a period of 10 minutes. Figure 1.4 shows the probability of complete tissue damage with respect to time when considering isothermal exposures at various temperatures. It indicates that at temperatures in excess of 60 °C, complete tissue damage occurs within a few seconds. For this reason, the 60 °C isotherm is a commonly used metric for assessing the zone of complete thermal damage induced by an ablation procedure.

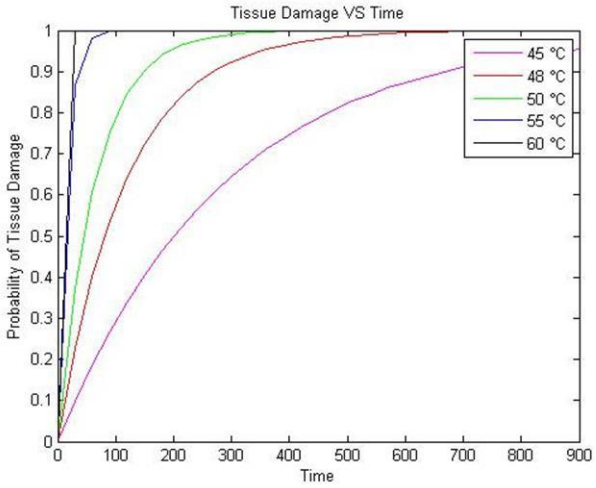

Figure 1.4. Tissue damage with progressing time

If a single antenna cannot provide a large enough ablation zone to treat a given tumor, multiple-antennas may be employed in an array. Laeseke *et al*. found that distributing power

amongst several antennas yields larger ablation zones than when using the same amount of power with a single antenna [9] as shown in Figure 1.5.

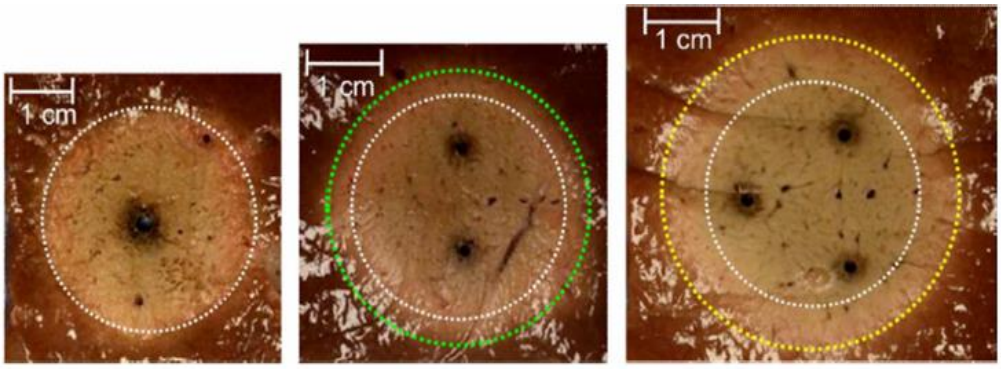

Figure 1.5. Single antenna and multiple antenna ablation [9]

As shown in Figure 1.6, multiple antennas may be employed in two configurations. The case where each antenna is powered by a single source is said to be operating in the synchronous mode of operation and the case where each antenna is powered by separate sources is said to be operating in asynchronous mode of operation.

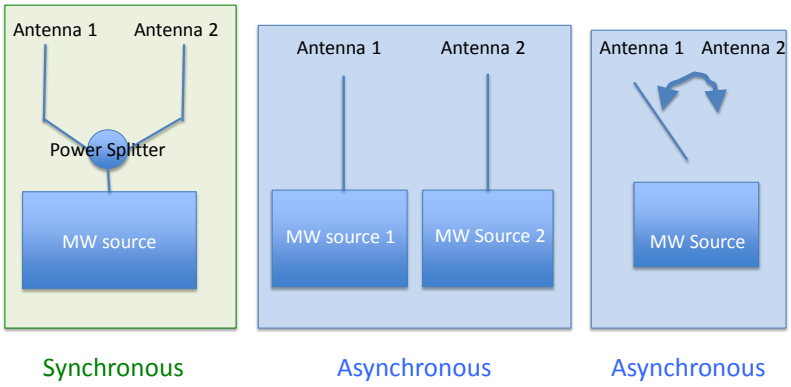

Figure 1.6. Setups for synchronous and asynchronous ablations operating in asynchronous mode.

Figure 1.7 shows the results of synchronous and asynchronous 915 MHz ablations for simulation and experiments from a literature study. It shows that synchronous operation with multiple antennas is able to produce larger ablation zones compared to asynchronous operation [10].

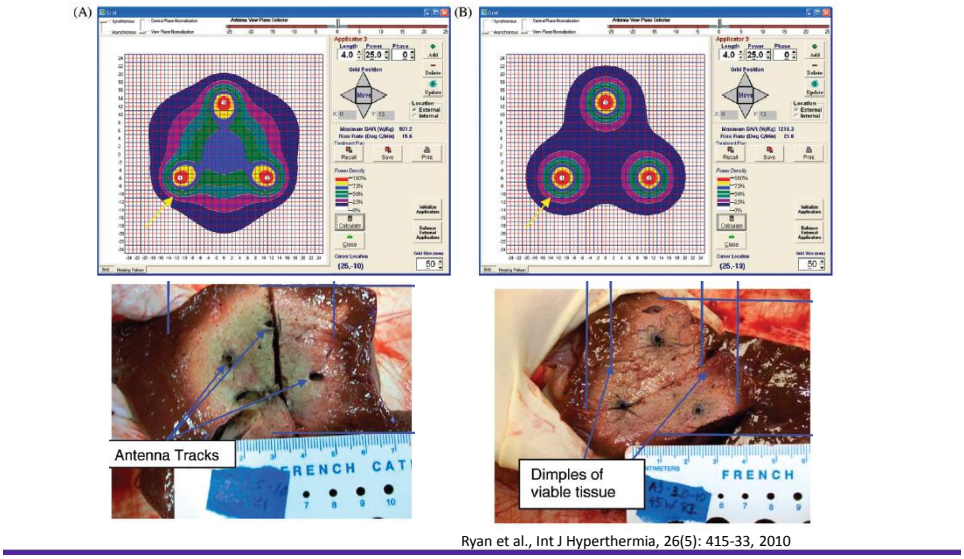

Figure 1.7. Experimentally and computationally measured ablation zones for synchronous and asynchronous ablations [10].

During a clinical ablation procedure, physicians rely on their experience and vendor-specifications of expected ablation zone outcomes to estimate treatment outcome. Figure 1.8 illustrates vendor-specified ablation geometry for a multiple-antenna ablation procedure. These specifications typically assume parallel antenna insertion to uniform depths, which may not always be possible during clinical procedures.

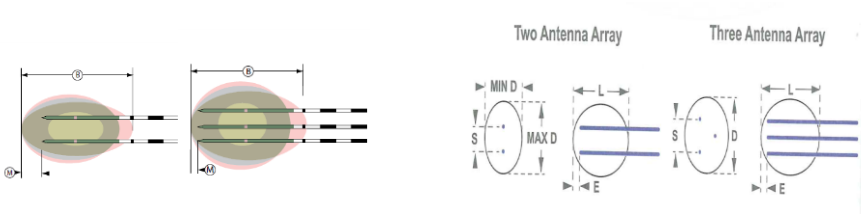

Covidien MW Ablation System BSD Medical MW Ablation System

Figure 1.8. Configurations provided by antenna manufacturing companies for performing microwave ablation.

The objective of this thesis is to characterize the impact of antenna mis-alignment on ablation outcome. Chapter 2 describes computational and experimental investigation of microwave ablation with non-parallel antennas at 915 MHz and 2.45 GHz. Chapter 3 discusses directions for potential future investigation.

CHAPTER 2: ANALYSIS OF NON-PARALLEL ANTENNA IMPLANTS FOR MICROWAVE ABLATION: IMPACT OF VARIATION IN FREQUENCY AND ANTENNA DESIGNS

Introduction

Thermal ablation is a minimally invasive treatment technique for destruction of localized, surgically unresectable tumors that is increasingly being used for treating tumors in the liver, lung, kidney, bone, and other organs [11], [12], [13]. Several energy modalities for heating tissues have been developed and are in clinical use, including radiofrequency currents, lasers, microwaves, ultrasound, and cryoablation. During ablation procedures, the goal is to raise the temperature of the target volume (tumor and a 5-10 mm margin of surrounding healthy tissue) to adverse temperatures in excess of 60 °C [14], leading to cell death by coagulative necrosis. The mechanism of heating during microwave ablation is the dielectric hysteresis of water and other polar molecules when exposed to a time-varying electromagnetic field.

Compared to other energy modalities, microwave ablation: produces higher temperatures, yields larger ablation volumes, is less susceptible to the impact of blood vessel heat sinks, does not require use of grounding pads, and has the ability to treat larger tumors by the use of multiple applicators simultaneously [7]. Single applicators are suitable for treating tumors of small dimensions (< 2 cm). For larger tumors, multiple applicators may be simultaneously employed, operating synchronously or asynchronously, to create large volume ablation zones [10]. Most currently available microwave ablation systems operate at frequencies of 915MHz and 2.45 GHz, which are both frequencies approved for industrial, scientific, and medical (ISM) use.

During multiple-applicator ablation, larger ablation zone volumes are achieved due to electromagnetic and thermal synergy between individual applicators. Synchronous operation of applicators enables phase interactions between the electric fields radiated by individual antennas, while asynchronous operation of applicators allows interaction of power deposited. A recent study with 915 MHz antennas indicated that larger ablation zones are achieved when multiple applicators are operated synchronously [10]. Multiple applicator heating with interstitial antennas has previously been extensively studied at lower frequencies and powers for hyperthermia applications [15], [16]. For synchronously operated systems, electromagnetic synergy is a function of the spacing between antennas and the wavelength of electromagnetic energy.

The expected ablation performance with a given configuration (number of antennas, applied power level, duration) is typically characterized with the extents of the ablation zone dimensions following experiments in unperfused *ex vivo* tissue. For multiple-antenna configurations, vendor specified ablation zones typically assume parallel applicator insertion to uniform depths. However, parallel insertion is not always possible due to anatomic constraints, imprecision of inserting flexible transmission cables with limited image guidance, and movement of the antenna and/or patient anatomy during the treatment process. Figure 2.1(a) illustrates antenna tip and insertion-point positions for six representative multiple-antenna ablation procedures performed at Rhode Island Hospital. For these six cases, none of the antenna implants were inserted in a parallel manner. An example non-parallel antenna insertion for a liver ablation procedure is shown in Figure 2.1(b). The impact of non-parallel insertion to non-uniform depths has not been previously studied for ablation applications.

For hyperthermia, Trembly *et al.* investigated the effects of variation of frequency and antenna length on the power deposition within a microwave antenna array of four parallel antennas

[15]. Their study showed that the greatest power deposition occurs at the center of an array with four antennas when the half wavelength of the dipole corresponds to the driving frequency. Clibbon *et al.* studied the impact of skewing one antenna on the SAR in an array of four antennas [16]. The results of their study showed that by skewing or varying the insertion depth of an antenna in an array of four antennas, the phase interaction between the applicators in the array is modified, thereby moving the location of maximum power deposition towards the periphery of the tumor instead of the tumor center. While several experimental studies have characterized multiple-applicator microwave ablation, these studies have only considered parallel antenna insertion to uniform depths [9], [10].

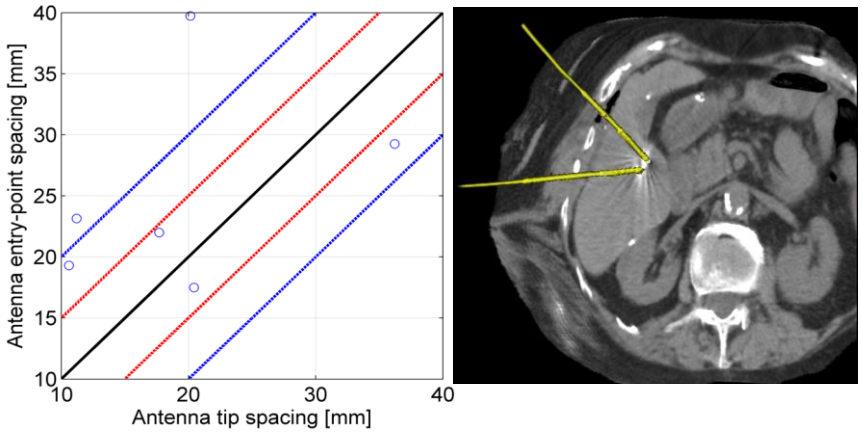

2.1 (a) 2.1 (b)

Figure 2.1 (a). shows the antenna entry-point and tip-spacing for six clinical multiple-antenna ablations. Parallel implants (black, solid line) are not routinely achieved. Figure 2.1(b) shows that parallel insertion is not always possible due to intervening anatomy (e.g. bone) and limited control of flexible antennas

The objective of this study is to: (1) volumetrically quantify the impact of non-parallel antenna insertion on temperature profiles and ablation zones during dual-applicator microwave ablation; and (2) assess the relationship between antenna operating frequency on the ablation

zone characteristics for non-parallel insertions. We employed 3D electromagnetic-thermal simulations and experiments in *ex vivo* tissue to characterize microwave ablation with non-parallel antenna implants. The results of this study suggests that there may be significant discrepancy between the expected ablation zones for non-parallel vs. parallel dual-antenna implants, particularly at 2.45 GHz. Section 2 describes the computational model, experimental procedure, and overall methodology carried out during this study. Results are presented in Section 3, followed by a discussion of the most important results in section 4.

Methods

In this study, we employed computational models to analytically compare the ablation zone shapes volumetrically for parallel and non-parallel antenna implants for different configurations. Heating experiments were performed in unperfused *ex vivo* tissue to validate the simulation results. Antenna implants consisted of synchronous, dual-antenna arrays, operating at either 915 MHz or 2.45 GHz.

Antenna Designs

We considered coaxial dipole antennas designed with the guidelines for resonant antenna length as described in [15]. Dipole antennas were selected since their design is simple, flexible and scalable for operation at different frequencies. However, their relatively long radiation pattern (along the antenna axis) and poor aspect ratio of ablation zones may not be practical for clinical applications intending to ablate tumors having spherical dimensions. To assess the impact of frequency of operation, we considered synchronously powered antennas at 915 MHz and 2.45 GHz. The effective antenna quarter-wavelength was calculated to be 28.1 mm for 915 MHz and 11.9 mm for 2.45 GHz. The effective wavelength incorporates the dielectric properties of the tissue load, as well as the insulating catheter, and their relative dimensions. For 2.45 GHz

ablations, we also considered a dual slot antenna [17], as it offers an improved antenna reflection coefficient, less heating along the length of the antenna, and a more spherical ablation zone. Figure 2.2 shows the geometry of the dipole and the dual slot antenna.

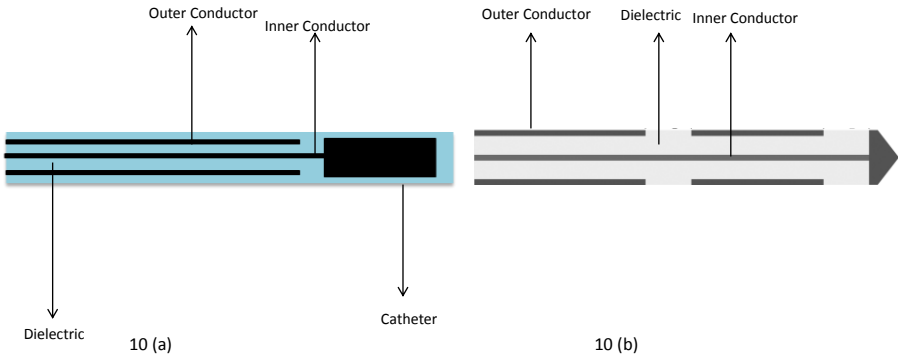

Figure 2.2. A Dipole Antenna 10 (a) and a Dual Slot Antenna 10 (b)

Figure 2.3 provides an illustration of the temperature profiles following 30 W, 10 min ablations for dipole and dual slot antennas at 2.45 GHz. The edge of the ablation zone is approximated using the 60 °C isotherm.

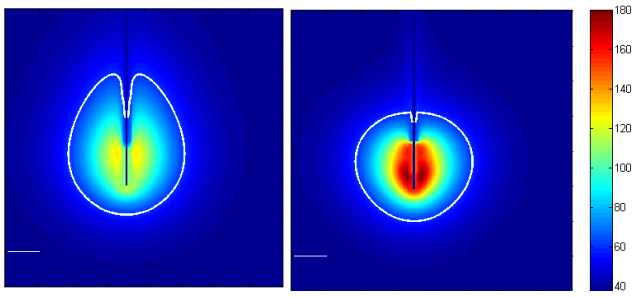

Figure 2.3. Temperature [°C] profile following 30 W, 10 min ablation with a single dipole antenna (left) and a dual slot antenna (right) tuned to 2.45 GHz.

Antenna configurations

For clinical multiple antenna microwave ablation procedures, the inter-antenna spacing range from 0.5 cm to 3.0 cm, with 1 – 2 cm spacing the most widely used [20],[21],[22]. In this

study, we considered synchronous, dual antenna implants with parallel antennas spaced 10 mm, 15 mm, and 20 mm apart. For each antenna spacing, we considered tip and feed (antenna entry point into tissue) displacements of 3 mm, 5 mm and 7.5 mm, creating converging and diverging configurations.

We used the Dice Similarity Coefficient (DSC) to compare the similarities between the ablation zones created by parallel and non-parallel antennas. The impact of non-parallel antenna insertion was quantified by comparing the similarity between the predicted ablation zone volume with the closest parallel case. The DSC was calculated using Equation 2

$$\mathrm{DSC} = \frac{2|A \cap B|}{(|A| + |B|)} \qquad (2)$$

where, A and B are the number of species in samples A and B, respectively. In this study, A and B represented binary maps for each voxel within the computational grid corresponding to 1 (tissue ablated, T > 60 °C) or 0 (tissue not ablated, T <= 60 °C). The value of DSC ranges between 0, indicating no similarity between A and B, and 1, indicating an identical match (or overlap) between A and B.

Computational Models

We employed 3D computational models of microwave propagation, energy deposition, and bioheat transfer to characterize dual-antenna microwave ablation. Figure 2.4 provides a block diagram representation of our computational model. In our computational models, we assumed static tissue properties with respect to temperature [23] and did not consider heterogeneous tissues.

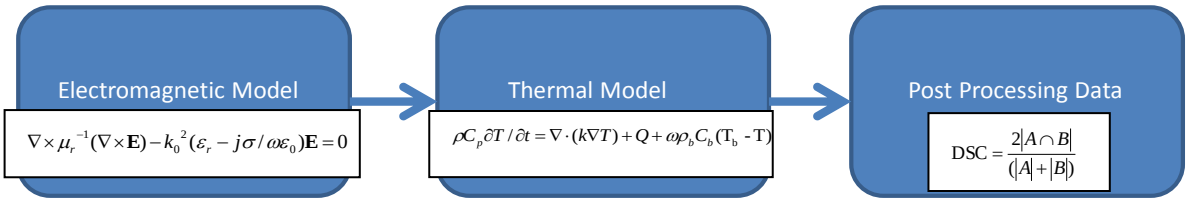

Figure 2.4. Block diagram representation of the computational model for estimating and comparing ablation zone profiles between parallel and non-parallel configurations

The electric field radiated into tissue during ablation was computed by solving the Helmholtz wave equation:

$$\nabla \times \mu_r^{-1}(\nabla \times \mathbf{E}) - k_0^2(\varepsilon_r - j\sigma/\omega\varepsilon_0)\mathbf{E} = 0 \qquad (3)$$

where, μ_r is the relative permeability, E is the electric field [V/m], k_0 is the wavenumber in free space [m^{-1}], ε_r is the relative permittivity, σ is the effective electrical conductivity [S/m], ω is the angular frequency of operation [s^{-1}], ε_0 is the permittivity of free space. A scattering boundary condition was employed on the edges of the computational domain to simulate the antenna as being inserted into an infinitely large volume of tissue. To ease computational burden, all copper regions were neglected from the computational domain and modeled with a perfect electric conductor boundary condition (i.e., $\sigma \rightarrow \infty$) [24], [25], [26]. The time-averaged power deposited in tissue was computed using:

$$Q = \frac{1}{2}\sigma|\mathbf{E}|^2 \qquad (4)$$

A transient bioheat equation including the perfusion term was used to model bioheat transfer in tissue.

$$\rho C_p \partial T/\partial t = \nabla \cdot (k\nabla T) + Q + \omega\rho_b C_b(T_b - T) \qquad (5)$$

where, ρ is the density [kg/m^3], C_p is the specific heat capacity of the medium [J/kg K], T is the temperature [K], t is time [s], k is the thermal conductivity [W/(m K)], Q is the heat source calculated from the electromagnetic model [W/m^3], ω is the blood perfusion rate [s^{-1}], ρ_b [kg/m^3] is the density of the blood, C_b is the specific heat capacity of the blood [J/kg K] and T_b [K] is the temperature of the blood in the surrounding arteries. Initial temperature in tissues was set to 37 °C. For validating the experimental results, a set of *ex vivo* simulations were performed by setting the perfusion term to zero. The 60 °C isotherm was used to estimate the extents of the ablation zones [14]. Material properties used for these simulations are listed in Table 2.1.

Property	**915 MHz**	**2.45 GHz**
Relative permittivity (ε_r)	46.76	43.03
Effective electrical conductivity (σ)	0.86 S/m	1.69 S/m
Thermal conductivity (k)	0.56 W/(m K)	
Density (ρ)	1060 kg/m^3	
Specific heat capacity (C_p)	3639 J/(kg K)	

Table 2.1. Material properties of liver tissue used in simulations

Experimental validation

Computational results were validated with dual antenna ablation experiments of select configurations in *ex vivo* tissue. Porcine muscle tissue was warmed up to ~35 °C in a

temperature-controlled bath. Antennas were inserted in parallel and converging configuration using a custom-designed template to guide antenna placement. For all dual antenna ablations, signal from an HP 8648C signal generator was amplified to 60 W using a microwave power amplifier (RF Core) and fed through an equal-phase splitter. Forward power during ablations was monitored at the input of the splitter with a Bird Electronic Corporation power meter to ensure 30 W was applied to each antenna. This experimental system represented ablation with synchronously powered antennas. The length and width of ablation zones were measured by observing the visibly discolored tissue. Figure 2.5 shows the block diagram of our experimental setup.

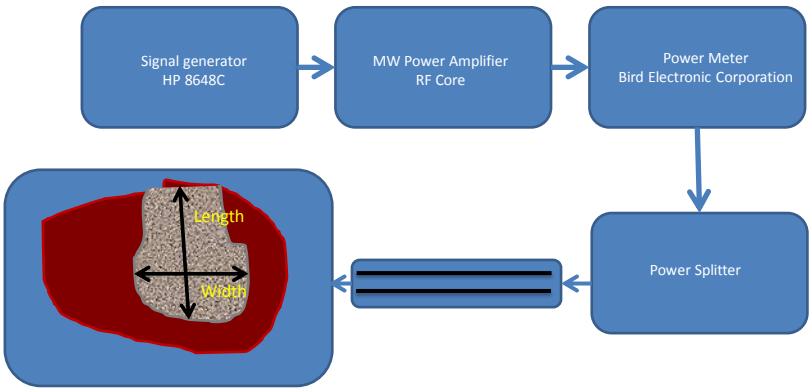

Figure 2.5. Block diagram representation of the experimental setup for determining ablation zone profiles

Results

Microwave ablation at 915 MHz and 2.45 GHz with dual dipole antennas

Table 2.2 details calculated DSC values to quantify the similarity between ablation zones obtained with 915 MHz and 2.45 GHz in converging configurations, compared to the closest parallel configuration. These data indicate that the discrepancies between ablation zones achieved with parallel vs. non-parallel configurations are more significant at 915 MHz, compared to 2.45 GHz. For both frequencies, the greatest discrepancy between parallel and converging dual-antenna arrays were observed for a nominal spacing of 20 mm. Figure 2.6 and 2.7 below show simulated ablation zones with 915 MHz and 2.45 GHz dipole antennas, respectively, spaced 20 mm apart in parallel and converging configurations.

Parallel spacing between antennas	915 MHz			2.45 GHz		
	Tip displacements for converging configurations			Tip displacements for converging configurations		
	3 mm	5 mm	7.5 mm	3 mm	5 mm	7.5 mm
10 mm	0.94			0.91		
15 mm	0.96	0.92		0.86	0.88	
20 mm	0.95	0.93	0.90	0.85	0.74	0.74

Table 2.2. Volumetric similarity (DSC) between parallel and converging dual-antenna configurations with tip displacements for 915 MHz and 2.45 GHz dipole antennas

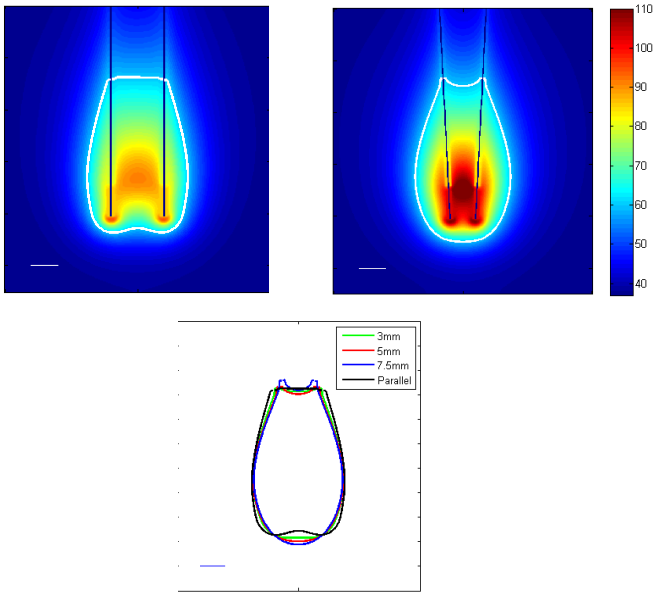

Figure 2.6. Temperature [°C] profiles and contour plot showing estimated extent of ablation zone following 10 min, 30 W/antenna dual-antenna ablation with 915 MHz coaxial dipole antennas in parallel and converging configurations.

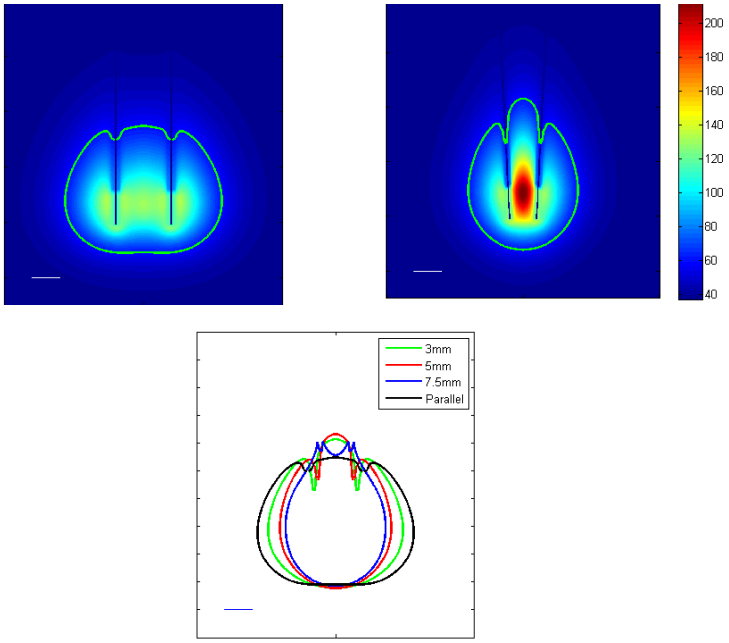

Figure 2.7. Temperature [°C] profiles and contour plot showing estimated extent of ablation zone following 10 min, 30 W/antenna dual-antenna ablation with 2.45 GHz coaxial dipole antennas in parallel and converging configurations.

Dual antenna ablation at 2.45 GHz for Dual Slot Antennas: Converging and Diverging Configurations

We conducted further simulations with 2.45 GHz dual-slot antennas, which afford more spherical ablation zones than dipole antennas. Tables 2.3 and 2.4 list calculated DSC values for dual-antenna arrays in converging and diverging configurations, respectively. Similar to the results observed for 2.45 GHz dipole antenna arrays, the ablation zone created by dual antenna arrays with 2.45 GHz dual-slot antennas are most sensitive to converging perturbations for a nominal spacing of 20 mm. For diverging perturbations, computed DSC values remain relatively large, suggesting only small changes in heating patterns compared to the parallel case.

Parallel spacing between antennas	Tip displacements for converging configurations		
	3 mm	5 mm	7.5 mm
10 mm	0.94		
15 mm	0.88	0.91	
20 mm	0.87	0.63	0.80

Table 2.3. Volumetric similarity between parallel and converging antenna configurations with tip displacements for dual slot antenna

Parallel spacing between antennas	Tip displacements for diverging configurations		
	3 mm	5 mm	7.5 mm
10 mm	0.87	0.79	0.73
15 mm	0.88	0.83	0.78
20 mm	0.93	0.88	0.79

Table 2.4. Volumetric similarity between parallel and diverging antenna configurations with tip displacements for dual slot antennas

Figure 2.8 shows simulated temperature profiles and ablation zones with 2.45 GHz dual slot antennas spaced 20 mm apart in converging configurations. The greatest discrepancy between the parallel configuration and converging configuration occurs for a perturbation of 5 mm/antenna. Interestingly, for greater perturbations, calculated DSC values and simulated ablation zone profiles are in closer agreement with the parallel case.

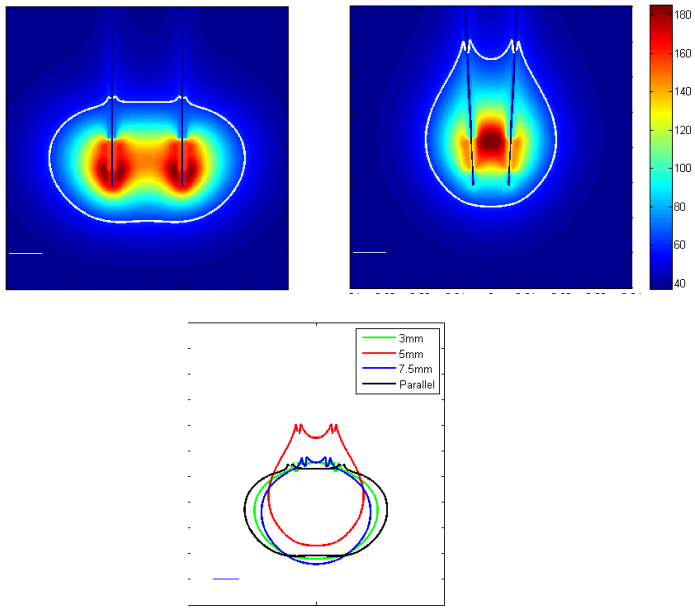

Figure 2.8. Temperature [°C] profiles and contour plot showing estimated extent of ablation zone following 10 min, 30 W/antenna dual-antenna ablation with 2.45 GHz dual-slot antennas in parallel and converging configurations.

To further investigate this, we simulated ablation with a single antenna in the vicinity of a second antenna that was not powered. The presence of another antenna caused electromagnetic interaction between the antenna applicators in such a way that the power deposition pattern for the 5 mm converging tip case shifts upwards compared to the parallel case Figure 2.9. Furthermore, the temperature profile abruptly falls off next to the unpowered antenna. This may be due to the fact that the electric field drops rapidly near the second antenna, acting as a reflector of incident electromagnetic energy from the powered antennas.

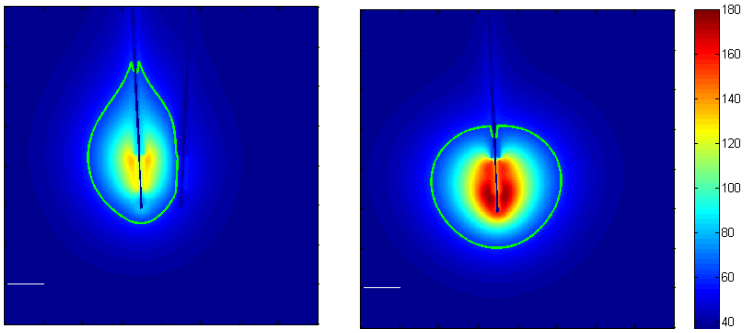

Figure 2.9. Temperature plot for the 20mm spacing 5mm converging case with only one antenna powered and temperature plot in presence of a single-dual slot antenna

Figure 2.10 shows simulated ablation zones with 2.45 GHz dual slot antennas spaced 20 mm apart in diverging configurations.

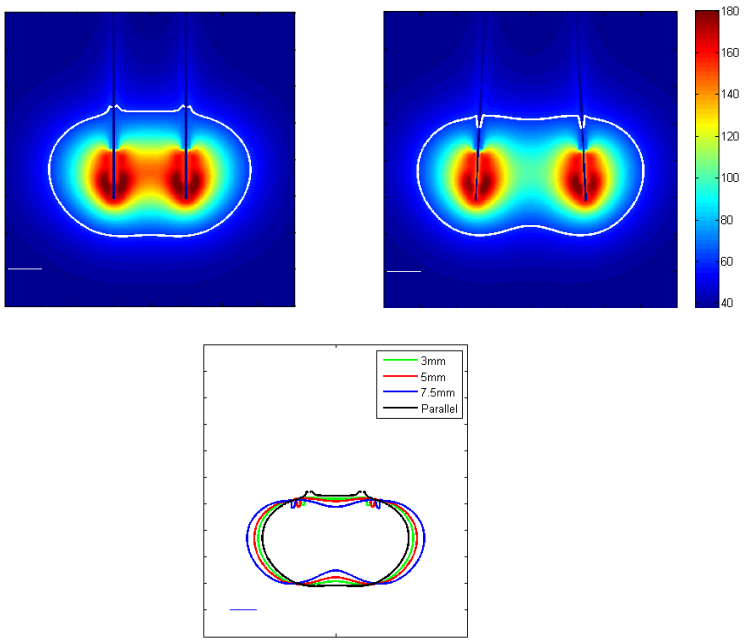

Figure 2.10. Temperature [°C] profiles and contour plot showing estimated extent of ablation zone following 10 min, 30 W/antenna dual-antenna ablation with 2.45 GHz dual-slot antennas in parallel and diverging configurations.

Microwave ablation at 915 MHz and 2.45 GHz with dual dipole antennas: In vivo ablation for elevated powers of 60 W per antenna

Parallel spacing between antennas	915 MHz			2.45 GHz		
	Tip displacements for converging configurations			Tip displacements for converging configurations		
	3 mm	5 mm	7.5 mm	3 mm	5 mm	7.5 mm
10 mm	0.95			0.91		
15 mm	0.97	0.94		0.88	0.90	
20 mm	0.96	0.94	0.92	0.87	0.77	0.70

Table 2.5. Volumetric similarity (DSC) between parallel and converging dual-antenna configurations with tip displacements for 915 MHz and 2.45 GHz dipole antennas for in vivo cases in the presence of blood perfusion

Table 2.5 above compares the volumetric similarity between the parallel and converging cases for dipole antennas operating at frequencies of 915 MHz and 2.45 GHz. Each antenna receives a power of 60 W. The trends of the results agree with the results for ex vivo cases.

Figure 2.11 and Figure 2.12 show the in vivo ablation cases with each antenna receiving a power of 60 W.

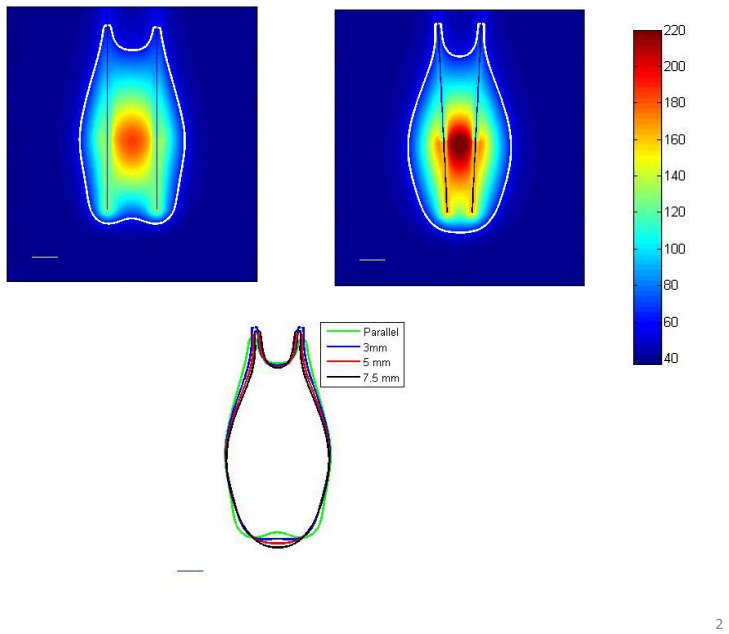

Figure 2.11. Temperature [°C] profiles and contour plot showing estimated extent of ablation zone following 10 min, 60 W/antenna dual-antenna ablation with 915 MHz dipole antennas in parallel and converging configurations.

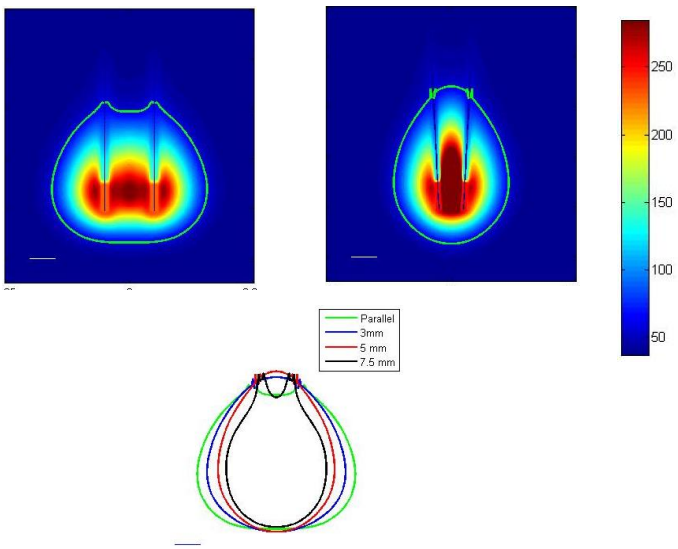

Figure 2.12. Temperature [°C] profiles and contour plot showing estimated extent of ablation zone following 10 min, 60 W/antenna dual-antenna ablation with 2.45 GHz dipole antennas in parallel and converging configurations.

Experimental validation

Figure 2.13 depicts ablation zones observed following heating experiments in *ex vivo* porcine muscle tissue using dual dipole antennas spaced 20 mm apart, tuned to 915 MHz and 2.45 GHz. The ablation zone profiles for dual-antenna parallel arrays (Figure 2.13, left column) are in good agreement with patterns predicted by simulations (Figure 2.6 and Figure 2.7). At 2.45 GHz, ablation with dual-antennas in a converging array (antenna tip-spacing = 10 mm; antenna feed-spacing = 20 mm) lead to increased heating along the antenna length, and reduced heating along the antenna short-axis, in agreement with simulations. At 915 MHz, experimental ablation zones with a converging array appeared shorter and wider, in contrast to predictions by simulations. This discrepancy may be due to the smaller insertion depth in *ex vivo* tissue, limited by the size of the tissue sample. Table 2.6 and Table 2.7 below show the ablation zone dimensions from the experimental procedures. The mean and standard deviations were calculated for the experiments.

Dual Antenna ablation with Dipole Antennas at 915 MHz for parallel configuration				Dual Antenna ablation with Dipole Antennas at 915 MHz for converging configuration with tips converging by 5 mm			
Width		Length		Width		Length	
Mean	Std	Mean	Std	Mean	Std	Mean	Std
3.93 cm	0.71 cm	5.94 cm	1.06 cm	3.90 cm	0.35 cm	6.37 cm	0.92 cm

Table 2.6. The mean and standard deviations of the experimental results at the operating frequency of 915 MHz.

Dual Antenna ablation with Dipole Antennas at 2450 MHz for parallel configuration				Dual Antenna ablation with Dipole Antennas at 2450 MHz for converging configuration with tips converging by 5 mm			
Width		Length		Width		Length	
Mean	Std	Mean	Std	Mean	Std	Mean	Std
4.36 cm	0.56 cm	4.38 cm	0.77 cm	3.99 cm	1.46 cm	5.03 cm	1.25 cm

Table 2.7. The mean and standard deviations of the experimental results at the operating frequency of 2.45 GHz.

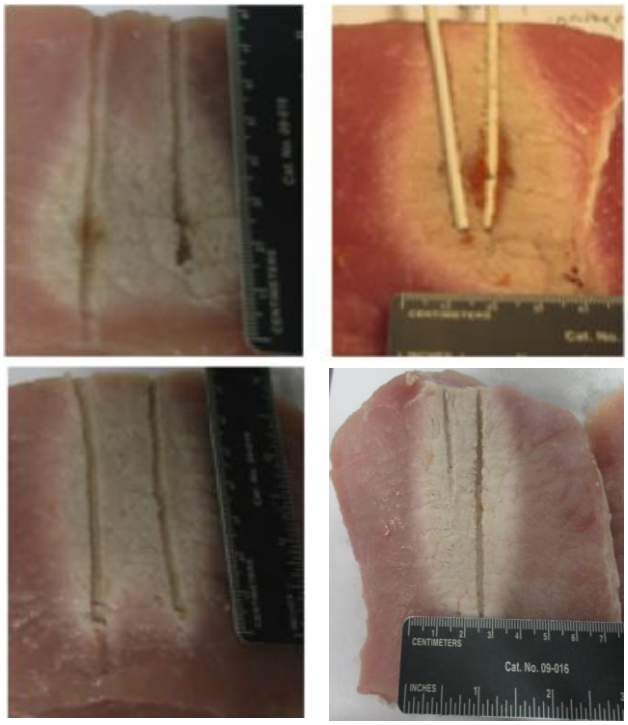

Figure 2.13. Experimentally observed ablation zone following dual-antenna ablations in ex vivo porcine tissue. (top left) 2.45 GHz, parallel and (top right) converging arrays. (Bottom left) 915 MHz parallel and (bottom right) converging arrays.

DISCUSSION

The objective of this study was to analyze the impact of non-parallel antenna insertion on the outcome of multiple antenna microwave ablation. A 3D FEM model based on Pennes bio-heat equation was implemented to compute power deposition and thermal profiles during abla-tion. We validated the simulation results by performing ablation experiments in *ex vivo* porcine muscle.

Dipole antennas produce elongated ablation zones as they heat along the axial length. In most practical cases of ablation large axial heating and a poor axial ratio leads to skin burns. Dual slot antennas are more realistic antenna designs in terms of offering spherical power deposition profiles with better aspect ratios. Figure 2.3 demonstrates this phenomenon appropriately by comparing the thermal profiles of dipole and dual slot antennas. The aspect ratio of the radiation pattern can be improved further by effective cooling of the antennas along the shaft [27].

For lower frequencies having larger wavelengths the impact of antenna misalignment on ablation zone characteristics is less compared to that for higher driving frequencies. The impact of antenna tip misalignment was observed to be less for the driving frequency of 915 MHz compared to that of 2.45 GHz. This may be attributed to the increase in electromagnetic wavelength with decreasing frequency. At 915 MHz the wavelength is a larger fraction of the distance between the antennas than at 2.45 GHz. The large wavelength mitigates the effect of variations caused by displacing antenna configurations as the perturbation is a smaller fraction of the wavelength. 20 mm spacing is equivalent to 1.68 wavelengths at 2.45 GHz compared to 0.712 wavelengths at 915 MHz. At 2.45 GHz with dipole antennas, the similarities between the parallel configuration and the converging configurations with tip displacement ranged from 0.74-

0.91, compared to 0.90-0.96 at 915 MHz.

The non-parallel cases compared to the parallel case when dipole antennas are used exhibit the estimated behavior that is with an increase in displacement of the antenna tips with respect to parallel configuration the similarity between the parallel and misaligned case decreases. However, for dual slot antennas spaced 20 mm apart this trend seems to be violated. When the tip displacement increases from 5 mm to 7.5 mm the similarity between the parallel and misaligned case increases instead of decreasing. This happens due to the fact that in the presence of the other antenna for 20 mm spacing between the antennas and 5 mm displacement the power deposition profile shifts upwards compared to the parallel case as a result of the electromagnetic interaction between the waves generated from the applicators. The same does not happen in the absence of the other antenna as demonstrated by Figure 2.9.

We noticed similar trends in the experimental results in terms of ablation zone profiles compared to our computational results. For the driving frequency of 915 MHz and parallel configuration the ablation zone was measured to be 5.94 cm (±1.06 cm) ×3.93 cm (±0.71 cm), for angled configuration with each of the tip converging by 5 mm the ablation zone was measured to be 6.37 cm (±0.92 cm) ×3.90 cm (±0.35 cm). For the driving frequency of 2450 MHz and parallel configuration the ablation zone was measured to be 4.38 cm (±0.77 cm) ×4.36 cm (±0.56 cm), for angled configuration with each tip converging by 5 mm the ablation zone was measured to be 5.03 cm (±1.25 cm) ×3.99 cm (±1.46 cm). The statistical differences between measured ablation zones for parallel and non-parallel case were found to be inconclusive and more experiments need to be repeated for getting a proper estimate of this difference.

In order to observe the impact in the presence of perfusion *in-vivo* computational models

were built using Pennes bioheat equation. We notice that blood perfusion acts as a heat sink which diminishes the dimensions of the ablation zone. With the same power supplied to the antennas there were several cases where the intratumoral temperatures were not even reaching the lower limits for tissue necrosis i.e. 60 °C. To counter the low temperatures the power supplied to each of the antennas were increased to 60 W. The result of *in-vivo* simulations with each antenna powered to 60 W agree with the trends observed for *ex-vivo* simulations with lower powers. It has been observed in literature previously that the presence of peritumoral vessels during ablation can act as a major heat sink causing inadequate heating of tumor tissues [28]. This often leads to recurrence of tumors especially for vessels (>3 cm). Thus, treatment planning should be used with higher power systems when vessels are present in the vicinity of the tumor tissues.

Similar to ablation using other modalities we observe that the addition of antennas did not impact the ablation zone dimensions along the axial length of the applicators. A possible disadvantage of this aspect is that due to the lack of control of heating pattern along the axial length of the applicators the temperatures in regions where the antennas are in close proximity to each other will be very high compared to temperatures in regions where the antennas are far away from each other [29].

This study provides ample evidence that contrary to the configurations provided by vendors non-parallel insertion of antennas can have a major impact on the power deposition profiles in tissues. Hence, proper treatment planning strategies need to be implemented based on actual needle positions and not based on arbitrary assumptions. Further research needs to be done to devise treatment planning systems for ablation of the target tissues.

CONCLUSION

Microwave ablation is increasingly being used for minimally invasive treatment of tumors in several organs. When targeting large volumes, multiple-antennas may be operated simultaneously, affording larger ablation zones due to electromagnetic and thermal synergy between applicators. Treatment planning during microwave ablation typically employs vendor specification of ablation zones based on experiments in *ex vivo* tissues. These experiments typically assume parallel insertion of antennas to uniform depths. This study was undertaken to investigate the impact of varying degrees of antenna misalignment on ablation outcome.

Our modeling and preliminary experimental results suggest that with increased displacement of the antenna tips the similarity of ablation zone compared to the parallel case decreases. Larger discrepancies between ablation zones created by parallel and non-parallel configurations were observed at 2.45 GHz compared to 915 MHz. We hypothesize that this may be due to the shorter electromagnetic wavelengths at 2.45 GHz. For 2.45 GHz dual-slot antennas spaced 20 mm apart, perturbations of 5 mm/antenna yielded greater dis-similarity of ablation zone compared to the parallel case than for 3 mm/antenna and 7.5 mm/antenna displacements. These results suggest that clinically observed ablation zones may be significantly different from vendor specifications when antennas are not in parallel configurations. Model-based patient-specific treatment plans may provide a more accurate estimate of expected ablation outcomes. To predict ablation zone profiles following multiple-antenna ablations, treatment planning calculations should incorporate actual antenna positions from images acquired following antenna placement. While this study considered coaxial dipole antennas since they can be readily scaled for various frequencies, future studies should consider more clinically relevant antennas. Finally, we intro-

duced a method for quantifying predicted ablation zone profiles incorporating uncertainty in antenna tip positions.

CHAPTER 3: CONCLUSION AND FUTURE WORK

Microwave ablation is an increasingly used modality for thermal therapy of surgically unresectable tumors. When treating large tumors, multiple antennas are employed simultaneously in array. Clinicians typically employ vendor-specifications of ablation zone to estimate or predict expected ablation outcome. This thesis was undertaken to assess the impact of non-parallel antenna insertion on ablation outcome.

Non-parallel antenna implants were found to be significantly different from the idealistic parallel implants in terms of the ablation zone dimensions. At present clinicians do not have a clear understanding of the physical interactions between applicators that are not aligned according to the configurations provided to them by antenna manufacturers. This study shows that there is a need for caution during such circumstances.

In the *ex-vivo* measurements we neglect the effect of blood perfusion and the change in tissue properties with respect to temperature. *In vivo* simulations are required for providing a better estimate of the impact of misalignment of antennas on the SAR. To generate an accurate model for ablation, presence of blood vessel, fatty tissues, and other sources of heterogeneity need to be considered, especially when they are in the vicinity of target tissues. Simulation results are based on the accuracy of the computational tools. Thus, to validate the accuracy of the simulation results there is a need for further in vivo experiments. Ex-vivo porcine tissue was used for experimental purposes to replicate some of the simulation results. It is difficult to replicate the *in-vivo* simulation results as experiments need to be done after euthanizing living animals. *In-vivo* methods are relatively expensive in terms of time, cost and animal lives compared to *ex-vivo* methods. Further investigation is warranted for analyzing the impact of non-ideal configurations under realistic situations.

REFERENCES

[1] R. Siegel, J. Ma, Z. Zou, and A. Jemal, "Cancer statistics, 2014: Cancer Statistics, 2014," *CA. Cancer J. Clin.*, vol. 64, no. 1, pp. 9–29, Jan. 2014.

[2] E. Kassner, "Evaluation and treatment of chemotherapy extravasation injuries," *J. Pediatr. Oncol. Nurs.*, vol. 17, no. 3, pp. 135–148, Jul. 2000.

[3] S. M. Bentzen, "Preventing or reducing late side effects of radiation therapy: radiobiology meets molecular pathology," *Nat. Rev. Cancer*, vol. 6, no. 9, pp. 702–713, Sep. 2006.

[4] A. Natale, E. Pisano, J. Shewchik, D. Bash, R. Fanelli, D. Potenza, P. Santarelli, R. Schweikert, R. White, W. Saliba, and others, "First human experience with pulmonary vein isolation using a through-the-balloon circumferential ultrasound ablation system for recurrent atrial fibrillation," *Circulation*, vol. 102, no. 16, pp. 1879–1882, 2000.

[5] Y. Feng and D. Fuentes, "Model-based planning and real-time predictive control for laser-induced thermal therapy," *Int. J. Hyperthermia*, vol. 27, no. 8, pp. 751–761, Dec. 2011.

[6] C. J. Simon, D. E. Dupuy, and W. W. Mayo-Smith, "Microwave Ablation: Principles and Applications1," *RadioGraphics*, vol. 25, no. suppl_1, pp. S69–S83, Oct. 2005.

[7] C. L. Brace, "Radiofrequency and Microwave Ablation of the Liver, Lung, Kidney, and Bone: What Are the Differences?," *Curr. Probl. Diagn. Radiol.*, vol. 38, no. 3, pp. 135–143, May 2009.

[8] I. A. Chang and U. D. Nguyen, "Thermal modeling of lesion growth with radiofrequency ablation devices," *Biomed. Eng. Online*, vol. 3, no. 1, p. 27, 2004.

[9] P. F. Laeseke, F. T. Lee Jr, D. W. van der Weide, and C. L. Brace, "Multiple-antenna microwave ablation: Spatially distributing power improves thermal profiles and reduces invasiveness," *J. Interv. Oncol.*, vol. 2, no. 2, p. 65, 2009.

[10] T. P. Ryan, P. F. Turner, and B. Hamilton, "Interstitial microwave transition from hyperthermia to ablation: Historical perspectives and current trends in thermal therapy," *Int. J. Hyperthermia*, vol. 26, no. 5, pp. 415–433, Aug. 2010.

[11] T. Livraghi, F. Meloni, M. Di Stasi, E. Rolle, L. Solbiati, C. Tinelli, and S. Rossi, "Sustained complete response and complications rates after radiofrequency ablation of very early hepatocellular carcinoma in cirrhosis: Is resection still the treatment of choice?," *Hepatology*, vol. 47, no. 1, pp. 82–89, Nov. 2007.

[12] D. A. Gervais, F. J. McGovern, B. J. Wood, S. N. Goldberg, W. S. McDougal, and P. R. Mueller, "Radio-frequency Ablation of Renal Cell Carcinoma: Early Clinical Experience 1," *Radiology*, vol. 217, no. 3, pp. 665–672, 2000.

[13] G. Abbas, A. Pennathur, R. J. Landreneau, and J. D. Luketich, "Radiofrequency and microwave ablation of lung tumors," *J. Surg. Oncol.*, vol. 100, no. 8, pp. 645–650, Dec. 2009.

[14] D. Yang, M. C. Converse, D. M. Mahvi, and J. G. Webster, "Measurement and Analysis of Tissue Temperature During Microwave Liver Ablation," *IEEE Trans. Biomed. Eng.*, vol. 54, no. 1, pp. 150–155, Jan. 2007.

[15] B. S. Trembly, "The effects of driving frequency and antenna length on power deposition within a microwave antenna array used for hyperthermia," *Biomed. Eng. IEEE Trans. On*, no. 2, pp. 152–157, 1985.

[16] K. L. Clibbon and A. McCowen, "Thermal modelling of nonideal interstitial microwave antenna array hyperthermia for the treatment of cancer," in *Microwave Symposium Digest, 1993., IEEE MTT-S International*, 1993, pp. 1147–1150.

[17] C. L. Brace, "Dual-slot antennas for microwave tissue heating: parametric design analysis and experimental validation," *Medical physics*, vol. 38, no. 7, pp. 4232–4240, 2011.

[18] M. M. Paulides, P. R. Stauffer, E. Neufeld, P. F. Maccarini, A. Kyriakou, R. A. M. Canters, C. J. Diederich, J. F. Bakker, and G. C. Van Rhoon, "Simulation techniques in hyperthermia treatment planning," *Int. J. Hyperthermia*, vol. 29, no. 4, pp. 346–357, Jun. 2013.

[19] C. L. Brace, P. F. Laeseke, L. A. Sampson, T. M. Frey, D. W. van der Weide, and F. T. Lee Jr, "Microwave Ablation with Multiple Simultaneously Powered Small-gauge Triaxial Antennas: Results from an in Vivo Swine Liver Model 1," *Radiology*, vol. 244, no. 1, pp. 151–156, 2007.
[20] F. Oshima, K. Yamakado, A. Nakatsuka, H. Takaki, M. Makita, and K. Takeda, "Simultaneous microwave ablation using multiple antennas in explanted bovine livers: relationship between ablative zone and antenna," *Radiat. Med.*, vol. 26, no. 7, pp. 408–414, Aug. 2008.
[21] N. C. Yu, D. S. Lu, S. S. Raman, D. E. Dupuy, C. J. Simon, C. Lassman, B. I. Aswad, D. Ianniti, and R. W. Busuttil, "Hepatocellular Carcinoma: Microwave Ablation with Multiple Straight and Loop Antenna Clusters—Pilot Comparison with Pathologic Findings 1," *Radiology*, vol. 239, no. 1, pp. 269–275, 2006.
[22] A. S. Wright, F. T. Lee, and D. M. Mahvi, "Hepatic Microwave Ablation With Multiple Antennae Results in Synergistically Larger Zones of Coagulation Necrosis," *Annals of Surgical Oncology*, vol. 10, no. 3, pp. 275–283, Apr. 2003.
[23] Z. Ji and C. L. Brace, "Expanded modeling of temperature-dependent dielectric properties for microwave thermal ablation," *Phys. Med. Biol.*, vol. 56, no. 16, pp. 5249–5264, Aug. 2011.
[24] C. Gabriel, S. Gabriel, and E. Corthout, "The dielectric properties of biological tissues: I. Literature survey," *Phys. Med. Biol.*, vol. 41, no. 11, p. 2231, 1996.
[25] S. Gabriel, R. W. Lau, and C. Gabriel, "The dielectric properties of biological tissues: II. Measurements in the frequency range 10 Hz to 20 GHz," *Phys. Med. Biol.*, vol. 41, no. 11, p. 2251, 1996.
[26] S. Gabriel, R. W. Lau, and C. Gabriel, "The dielectric properties of biological tissues: III. Parametric models for the dielectric spectrum of tissues," *Phys. Med. Biol.*, vol. 41, no. 11, p. 2271, 1996.
[27] M. Kuang, M. D. Lu, X. Y. Xie, H. X. Xu, L. Q. Mo, G. J. Liu, Z. F. Xu, Y. L. Zheng, and J. Y. Liang, "Liver Cancer: Increased Microwave Delivery to Ablation Zone with Cooled-Shaft Antenna—Experimental and Clinical Studies 1," *Radiology*, vol. 242, no. 3, pp. 914–924, 2007.
[28] D. S. K. Lu, S. S. Raman, P. Limanond, D. Aziz, J. Economou, R. Busuttil, and J. Sayre, "Influence of Large Peritumoral Vessels on Outcome of Radiofrequency Ablation of Liver Tumors," *J. Vasc. Interv. Radiol.*, vol. 14, no. 10, pp. 1267–1274, Oct. 2003.
[29] P. Prakash, V. A. Salgaonkar, E. C. Burdette, and C. J. Diederich, "Multiple applicator hepatic ablation with interstitial ultrasound devices: Theoretical and experimental investigation," *Med. Phys.*, vol. 39, no. 12, pp. 7338–7349, 2012.